Journal of ELECTRONIC MATERIALS, Vol. 43, No. 4, 2014
DOI: 10.1007/s11664-013-2951-y

Preparation of TiO_2(B) Nanosheets by a Hydrothermal Process and Their Application as an Anode for Lithium-Ion Batteries

HSIN-YI WU,[1] MIN-HSIUNG HON,[1,2] CHI-YUN KUAN,[1] and ING-CHI LEU[3,4]

1.—Department of Materials Science and Engineering, National Cheng Kung University, Tainan 701, Taiwan. 2.—Research Center for Energy Technology and Strategy, National Cheng Kung University, Tainan 701, Taiwan. 3.—Department of Materials Science, National University of Tainan, Tainan 701, Taiwan. 4.—e-mail: icleu@mail.mse.ncku.edu.tw

TiO_2 nanosheets with single monoclinic phase have been synthesized by a hydrothermal method using 6 M NaOH aqueous solution at 180°C. TiO_2 nanosheets exhibited surface area of 100 $m^2\ g^{-1}$, which is larger than those obtained by solid-state reaction. The capability of lithium-ion batteries could be strongly enhanced by TiO_2(B) nanosheets to yield discharge capacity higher than 200 mAh g^{-1}, even upon 25 cycles of 0.1-C-rate discharge–charge operations, showing highly reversible capacity and good cycling stability with excellent capacity retention of 96% with water-based binder. The results suggest that TiO_2(B) nanosheets could be a promising negative electrode material for use in lithium-ion batteries.

Key words: TiO_2(B) nanosheets, hydrothermal synthesis, Li-ion batteries

INTRODUCTION

Nanometer-sized electrochemically active materials as the electrode of lithium rechargeable batteries, compared with micrometer-sized materials, have attracted much attention due to the fast transport of lithium-ion species facilitated by a shorter diffusion length. Nanomaterials can play an important role in improving the performance of lithium-ion batteries, because in nanomaterial systems the distances over which Li^+ must diffuse are dramatically decreased, nanomaterials can quickly absorb and store vast numbers of lithium ions without any deterioration in the electrode, and nanomaterials have large surface areas, short diffusion lengths, and fast diffusion rates along their many grain boundaries.[1–6] Several potential advantages associated with the development of nanoelectrodes for lithium-ion batteries could be summarized as follows: (i) better accommodation of the strain of lithium insertion/extraction for improved cycle life, (ii) higher electrode/electrolyte contact area leading to higher charge/discharge rates, and (iii) short path lengths for both electron and Li^+ transport. Based on these advantages, efforts have been devoted to explore negative and positive nanostructured electrode materials for lithium-ion battery applications.[7,8]

Of the various crystal systems of TiO_2, both the rutile tetragonal crystal system and brookite orthorhombic crystal system can accommodate only small amounts of lithium, while the anatase tetragonal crystal system and TiO_2(B) monoclinic crystal system have higher ratios of lithium insertion.[9] Monoclinic titania, commonly named TiO_2(B) phase (a metastable polymorph of titanium dioxide), has a relatively open structure with significant voids and continuous channels, facilitating lithium intercalation and leading to excellent electrochemical properties.[10–15] Also, TiO_2(B) is the least dense polymorph of TiO_2, which makes it a superior intercalation host for lithium as compared with rutile and anatase.[16]

Herein, facile hydrothermal synthesis of monoclinic crystal system TiO_2 nanocrystallites is reported. The effect of the NaOH concentration on the preparation of TiO_2 nanostructures and their structural and morphological features and electrochemical properties have been studied using x-ray diffraction (XRD)

(Received August 6, 2013; accepted December 11, 2013; published online January 23, 2014)

analysis, transmission electron microscopy (TEM), Brunauer–Emmett–Teller (BET) analysis, galvanostatic cycling, and cyclic voltammetry (CV). The TiO_2(B) nanosheets were also tested as an anode material for use in lithium-ion batteries, presenting high reversible capacity and good cycling performance, which indicates promising applications as anode materials for rechargeable lithium-ion batteries.

EXPERIMENTAL PROCEDURES

Sample Preparation and Characterization

The TiO_2 source used for preparing the nanosheets was commercially available TiO_2 powder (P25, anatase and rutile phases in ratio of about 3:1; Evonik-Degussa GmbH, Essen, Germay). TiO_2 nanosheets were hydrothermally synthesized from a mixture of TiO_2 powder (P25), sodium hydroxide (NaOH), and deionized (DI) water. The mixture was first treated with stirring for 30 min, followed by heating at 180°C in a Teflon-lined autoclave for 12 h. After reaction, the sample was rinsed with 10 M hydrochloric acid (HCl) solution until a pH value of about 7.5 was reached; the precipitate obtained by centrifugation was rinsed with DI water, then dried at 65°C for 12 h. The effects of different concentrations of NaOH on the preparation of TiO_2 nanosheets were studied. The prepared samples were characterized using XRD (Cu K_α, λ = 1.54178 Å; Rigaku, Tokyo, Japan), BET (ASAP 2010; Micromeritics, Norcross, GA), and TEM (JEM-2100F; JEOL, Tokyo, Japan) analysis.

Electrode Preparation and Electrochemical Characterization

The working electrode was composed of active material (TiO_2 nanosheets), conductive agent (carbon black, super-P-Li), and water-based binder [poly-acrylic acid (PAA)] in weight ratio of 67:22:11. This mixture was coated uniformly onto a copper foil. Lithium metal was used as the counter and reference electrodes. $LiPF_6$ (1 M) in ethylene carbonate (EC)/dimethyl carbonate (DMC) at volume ratio of 1:1 was used as the electrolyte (LIPASTE-EDEC/PF1; Tomiyama Pure Chemical Industry, Japan). To examine the redox characteristics of such a TiO_2 anode in a lithium-ion battery, CV analysis was carried out using a potentiostat (model 263A; EG&G) at scan rate of 0.5 mV s^{-1} in the potential range of 1.0 V to 3.0 V. The battery was subjected to galvanostatic charge–discharge tests using battery test equipment (Arbin Inc., USA). In these tests, the applied charge–discharge potentials were in the range from 1.0 V to 3.0 V, the charge/discharge rate was set to 0.1 C, and the temperature was maintained at room temperature.

RESULTS AND DISCUSSION

TiO_2 nanosheets were first reported by Kasuga et al.[17,18] through the reaction of TiO_2 particles with NaOH aqueous solution. Figure 1 shows the nanostructured morphology of TiO_2 synthesized using 3 M, 4.7 M, and 6 M NaOH aqueous solutions at 180°C for 12 h and dried at 65°C for 12 h. It can be seen that the fraction of nanosheets in the product could be enhanced by increasing the NaOH concentration, and their edges rolled up due to surface tension (Fig. 1c).[19,20] According to previous research,[19,21–24] this morphological development is due to layered-structured titanates such as $Na_xTi_yO_z$ that can be formed as intermediate products when TiO_2 is treated with NaOH by a hydrothermal process. During the hydrothermal process, Na^+ cations residing between edge-shared TiO_6 octahedral layers can gradually be replaced by H_2O molecules[25,26] (as shown in Fig. 2, Eq. 1). Intercalated H_2O molecules are larger than Na^+ ions, so the interlayer distance increases and the static interaction between neighboring TiO_6 octahedral sheets weakens. Consequently, layered titanate particles exfoliate to form nanosheets that curl up from the edges to form TiO_2 nanosheets[27–29] (as shown in Fig. 2, Eqs. 2, 3). Figure 1b shows intermediate products that exhibit particle and sheet structures, with several edges of the nanosheet structures rolling up. Figure 2 shows a schematic of the TiO_2 nanostructure formation via alkali hydrothermal synthesis; various forms of titanates can be formed, possibly having a layered structure.

Figure 3 shows the XRD patterns of the products synthesized using different concentrations of NaOH solution (3 M, 4.7 M, and 6 M), and the original P25 powder for comparison. As is well known, the diffraction patterns of P25 show it to be composed of anatase and rutile, with the main phase being anatase.[21] On increasing the NaOH concentration to 6 M, the diffraction pattern of the reaction product could be indexed to the monoclinic titanium oxide phase [TiO_2(B)] according to Joint Committee on Powder Diffraction Standards (JCPDS) card no. 74-1940. Under 3 M and 4.7 M solution conditions, the main diffraction patterns were similar to the original P25 powder. From the TEM images, products in the form of particles and nanosheets are synthesized in 3 M and 6 M NaOH aqueous solutions, respectively. Moreover, the XRD diffraction patterns correspond to pure anatase and monoclinic phase for 3 M and 6 M solutions, respectively. According to the discussion above, it is suggested that the nanostructure morphologies exhibiting particles and sheets can have different phase structures, as shown in Fig. 1b. To confirm the phase structure, the electron diffraction technique was applied to identify the reaction product, as shown in the inset of Fig. 1b. The results imply that the particle and nanosheet morphologies correspond to the anatase and monoclinic phase structures, respectively. However, the TEM morphology of the product synthesized using NaOH concentration of 4.7 M (Fig. 1b) shows the particle and sheet nanostructure, but the XRD pattern does not have peaks

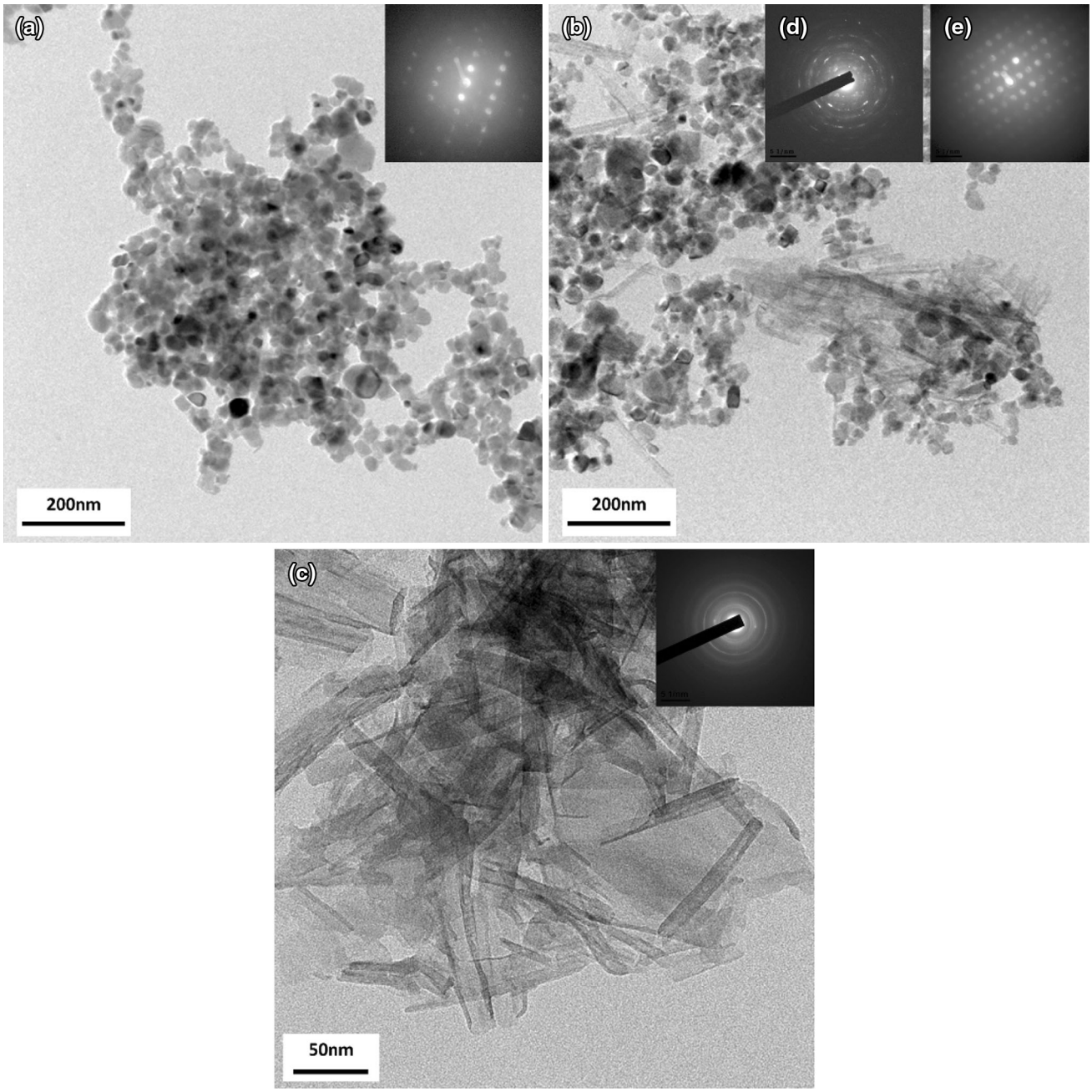

Fig. 1. TEM images and selected-area electron diffraction (SAED) patterns of TiO_2 nanostructures produced by alkaline hydrothermal treatment with different NaOH concentrations of (a) 3 M, (b) 4.7 M, and (c) 6 M. Inset: SAED patterns taken from (d) nanosheet and (e) nanoparticle.

similar to the 6 M product. It may be too weak compared with that for the concentration of 6 M. As reported in the literature,[19,20,22] researchers took a long time (24 h or more) to prepare nanosheet structures, while a shorter time was used in the present study. In other words, the pure monoclinic phase with high surface area could be obtained in a short time through a facile process.

N_2 adsorption–desorption isotherm analysis was used to measure the surface area. Figure 4 shows the specific surface areas of TiO_2 synthesized using different NaOH concentrations. Through BET measurements, the areas for 0 M, 3 M, 4.7 M, and 6 M were found to be 50 $m^2 g^{-1}$, 55 $m^2 g^{-1}$, 70 $m^2 g^{-1}$, and 100 $m^2 g^{-1}$, respectively. These results illustrate that the surface area can be increased by increasing the NaOH concentration used in the hydrothermal synthesis. In other words, the surface area increases with the morphological development from particles to two-dimensional nanosheets. The obtained TiO_2(B) nanosheets have higher specific surface areas than obtained with other parameters (P25, 3 M, and 4.7 M). These results imply that higher surface areas would have higher electrode–electrolyte

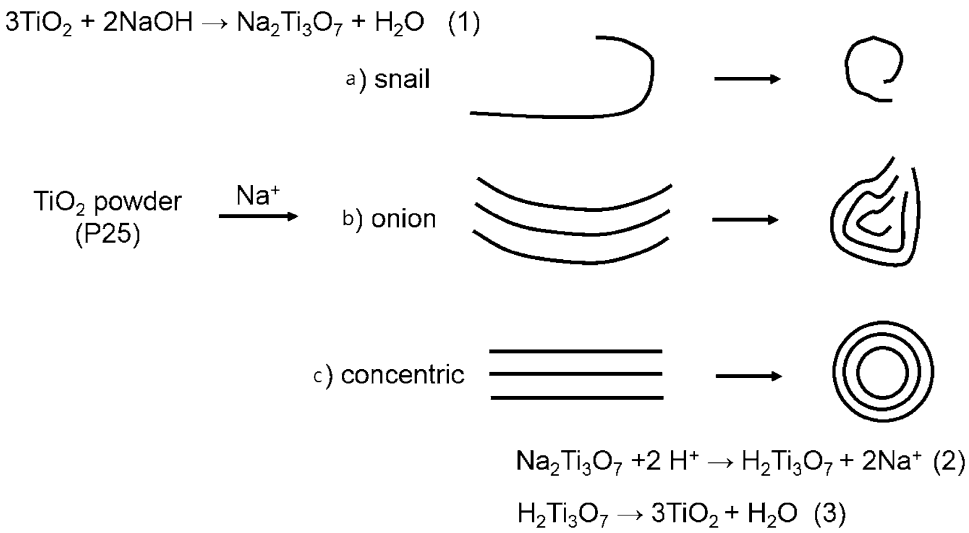

Fig. 2. Possible formation mechanisms for multiwalled nanotubes and the nature of the products: (a) helical scrolling of a single-layer nanosheet, (b) curving of several conjoined nanosheets or (c) direct production of a multiwalled nanotube.

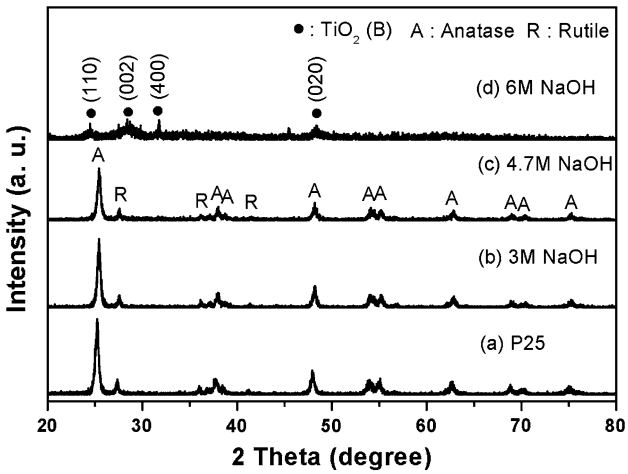

Fig. 3. x-Ray diffraction patterns of original TiO_2 (P25 powder) and TiO_2 nanostructures obtained by the hydrothermal method with different NaOH concentrations.

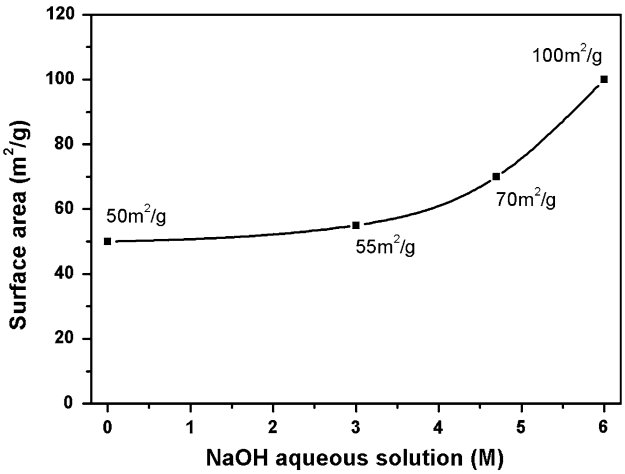

Fig. 4. BET surface areas of TiO_2 nanostructures synthesized by hydrothermal reaction with different NaOH concentrations.

contact areas, shorter diffusion paths into the lattice, and reduced strain of intercalation, and the cycling performance could be improved.

A comparison of the battery characteristic for high-surface-area nanosheets and other parameters is shown in Fig. 5, which presents the specific charge–discharge capacity and cyclic voltammograms (CVs) for P25, TiO_2 nanostructures (3 M and 4.7 M), and TiO_2(B) nanosheets (6 M) between 3 V and 1 V at a rate of 0.1 C and scan rate of 0.5 mV s^{-1} for potential between 1.0 V and 3.0 V. P25 shows a large irreversible capacity of 245.9 mAh g^{-1} (Fig. 5a1) in the first cycle, which is attributed to the formation of a solid electrolyte interphase (SEI) film during the discharge process. TiO_2(B) nanosheets show a higher discharge capacity of 229 mAh g^{-1} than that of P25 (162 mAh g^{-1}) for the 3 M and 4.7 M concentrations. The TiO_2(B) nanosheets with high surface area (100 m^2 g^{-1}) could create more adsorptive and reactive sites to accelerate reactions. The rate of the insertion and extraction processes could be promoted, and a higher capacity could be obtained. This could also result in a lower charge density for sufficient space decentralizing electrons and holes on the surface, leading to restrained surface recombination.[30] However, the curve for the TiO_2(B) nanosheets (Fig. 5d1) shows a smooth slope without any potential plateau, and the smoothly sloping property of the voltage profiles indicates that lithium intercalation into the nanosheets remains a single-phase process after repeated cycling, which means that there is no two-phase interface during the lithium intercalation process.[31]

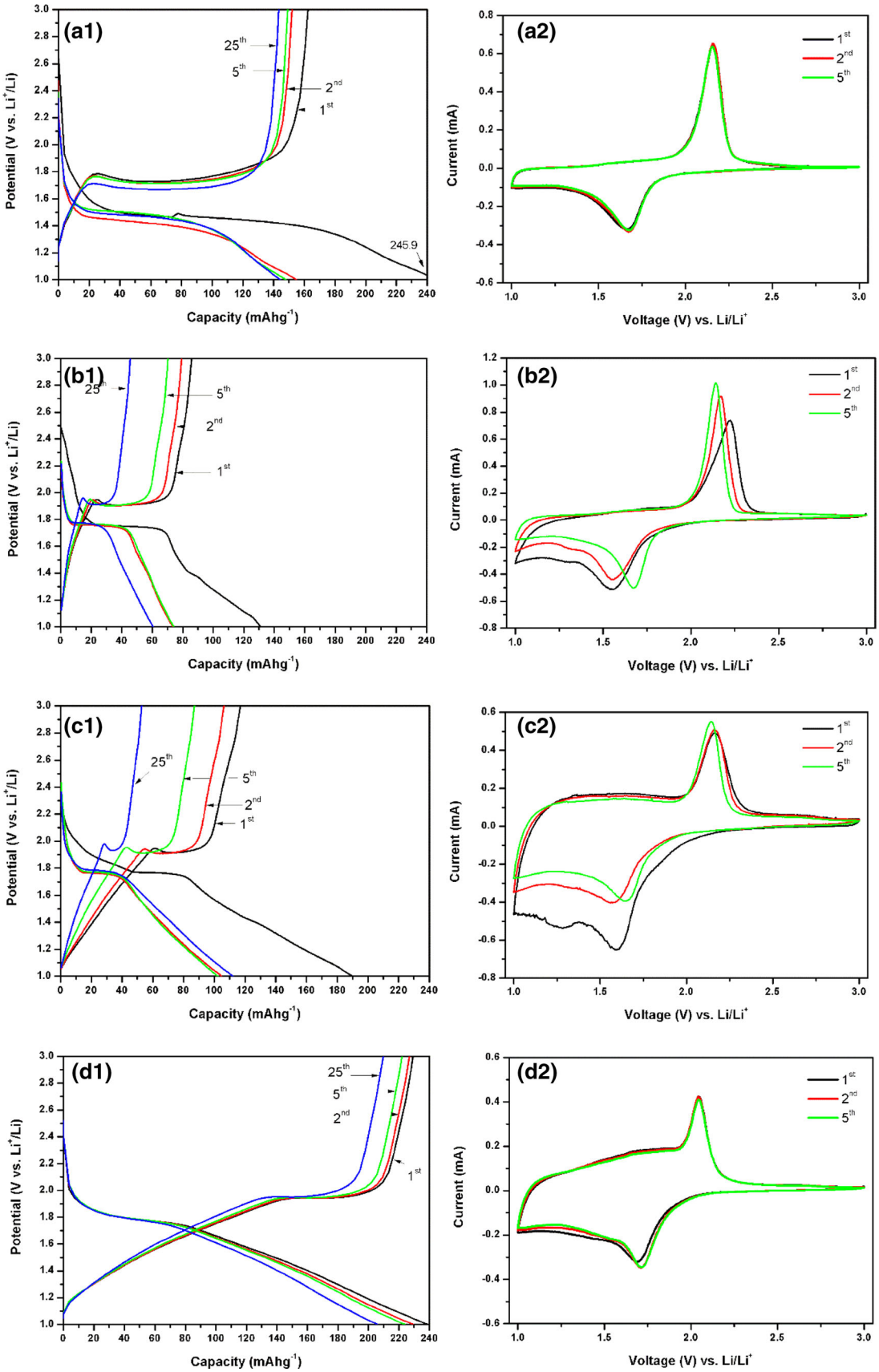

Fig. 5. Capacity–voltage profiles and representative CV for (a1, a2) original P25, and TiO_2 nanostructures synthesized by hydrothermal reaction with different NaOH concentrations of (b1, b2) 3 M, (c1, c2) 4.7 M, and (d1, d2) 6 M at scan rate of 0.5 mV s^{-1} between 1 V and 3 V.

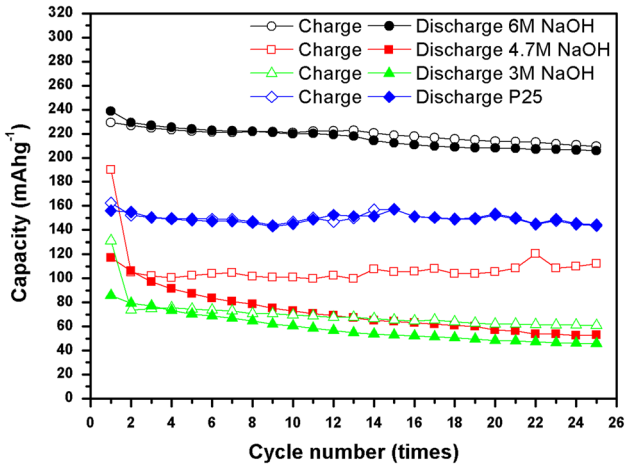

Fig. 6. Cycle performance at 0.1 C rate for original P25 and TiO_2 nanostructures synthesized by hydrothermal reaction using different NaOH concentrations.

At the scan rate of 0.5 mV s^{-1}, the oxidation and reduction current peaks result from the overall cell reaction for Li^+ insertion/extraction for TiO_2 or TiO_2(B). The related reactions are as follows:

$$TiO_2 + xLi^+ + xe^- \Leftrightarrow Li_xTiO_2$$

$$TiO_2(B) + xLi^+ + xe^- \Leftrightarrow Li_xTiO_2(B).$$

Figure 5a2–d2 demonstrates the behavior of the Li^+ insertion/extraction processes for the TiO_2 electrode. The voltage positions of the initial cycle are similar, at about 1.70 V and 2.10 V, which is in accordance with the pair of peaks reported for TiO_2.[16,31] It can be seen that the electrochemical properties of the four materials are quite different. Figure 5d2 shows a small irreversible capacity and relatively little difference between the first, second, and third cycles. This phenomenon could be explained by the fact that the TiO_2(B) nanosheets have freely accessible parallel channels, which follow the [001] direction, in which lithium ions can be accommodated without any remarkable distortion of the structure,[32] as well as the surface free energy of the overall Li insertion process and the differences in the structural strains associated with lithium insertion/extraction, compared with bulk counterparts.[20,33]

Compared with recent reports using different TiO_2 electrodes, such as nanosheets,[19] nanotubes,[20,34] nanoneedles,[35] and nanowires,[36] it is interesting to find that their cycle life performance did not show better capacity retention. However, in the present study, the capacity of the TiO_2(B) nanosheets could be maintained after 25 cycles, i.e., at 96%, as shown in Fig. 6. The crystal structure is that of TiO_2(B), a polymorph of titanium dioxide composed of edge- and corner-sharing TiO_6 but with a slightly lower density than rutile, anatase or brookite, so the Li^+ in TiO_2(B) exhibits better diffusion. It is suggested that TiO_2(B) nanosheets are a promising host material for use in lithium batteries owing to their open structure with large surface area and their provision of ideal pathways for rapid incorporation and diffusion of Li^+ in the nanosheets.

CONCLUSIONS

TiO_2 nanostructures were synthesized through a simple alkaline hydrothermal reaction by tuning the NaOH concentration. The morphology, crystalline phase, specific surface area, and electrochemical behaviors were characterized. TiO_2 of single monoclinic phase was successfully synthesized in 6 M NaOH at 180°C for 12 h, exhibiting a large surface area (100 m^2 g^{-1}). Moreover, TiO_2(B) nanosheets showed highly reversible capacity and good cycling stability with excellent capacity retention of 96% after 25 cycles and reversible capacity of 209 mAh g^{-1}. TiO_2(B) demonstrates lithium storage kinetics governed by a pseudocapacitive faradaic process, which is not limited by solid-state diffusion of Li ions. Such TiO_2(B) with open structure can facilitate lithium transport and effectively buffer the volume changes during lithium ion intercalation/deintercalation. The excellent capacity indicates that nanostructured TiO_2(B) is suitable for use as an anode material in lithium-ion batteries.

ACKNOWLEDGEMENT

This study was supported by the National Science Council of Taiwan, Republic of China (NSC 100-2221-E-006-123-MY3 and NSC 100-2628-E-024-001-MY2), which is greatly appreciated.

REFERENCES

1. Y.G. Guo, J.S. Hu, and L.J. Wan, *Adv. Mater.* 20, 2878 (2008).
2. C.H. Jiang, E. Hosono, and H.S. Zhou, *Nano Today* 1, 28 (2006).
3. Y. Yu, X. Wang, H. Sun, and M. Ahmad, *RSC Adv.* 2, 7901 (2012).
4. J.S. Chen and X.W. Lou, *Mater. Today* 15, 246 (2012).
5. J. Chen, L. Yang, S. Fang, and Y. Tang, *Electrochim. Acta* 55, 6596 (2010).
6. X. Wang, Q. Xiang, B. Liu, L. Wang, T. Luo, D. Chen, and G. Shen, *Sci. Rep.* 3, 2007 (2013).
7. J.H. Lee, M.H. Hon, Y.W. Chung, and I.C. Leu, *Appl. Phys. A* 102, 3 (2011).
8. S. Arico, P. Bruce, B. Scrosati, J.M. Tarascon, and W.V. Schalkwijk, *Nat. Mater.* 4, 366 (2005).
9. D.W. Murphy, R.J. Cava, S.M. Zahurak, and A. Santoro, *Solid State Ion.* 413, 9 (1983).
10. A.R. Armstrong, G. Armstrong, J. Canales, and P.G. Bruce, *Angew. Chem. Int. Ed.* 43, 2286 (2004).
11. G. Armstrong, A.R. Armstrong, J. Canales, and P.G. Bruce, *Chem. Commun.* 19, 2454 (2005).
12. A.R. Armstrong, G. Armstrong, J. Canales, R. Garcia, and P.G. Bruce, *Adv. Mater.* 17, 862 (2005).
13. J. Zhu, J. Zhang, F. Chen, and M. Anpo, *Mater. Lett.* 59, 3378 (2005).

14. G. Wang, Q. Wang, L. Wu, and J. Li, *J. Phys. Chem. B* 110, 22029 (2006).
15. X. Su, Q.L. Wu, X. Zhan, J. Wu, S. Wei, and Z. Guo, *J. Mater. Sci.* 47, 2519 (2012).
16. G. Armstrong, A.R. Armstrong, J. Canales, and P.G. Bruce, *Electrochem. Solid State Lett.* 9, A139 (2006).
17. T. Kasuga, M. Hiramatsu, A. Hoson, T. Sekino, and K. Niihara, *Adv. Mater.* 11, 1307 (1999).
18. T. Kasuga, M. Hiramatsu, A. Hoson, T. Sekino, and K. Niihara, *Langmuir* 14, 3160 (1998).
19. G. Xiang, T. Li, J. Zhuang, and X. Wang, *Chem. Commun.* 46, 6801 (2010).
20. M.G. Choi, Y.G. Lee, S.W. Song, and K.M. Kim, *Electrochim. Acta* 55, 5975 (2010).
21. D.V. Bavykin, V.N. Parmon, A.A. Lapkin, and F.C. Walsh, *J. Mater. Chem.* 14, 3370 (2004).
22. Z. Chang, J. Liu, J. Liu, and X. Sun, *J. Mater. Chem.* 21, 277 (2011).
23. N. Masaki, S. Uchida, H. Yamane, and T. Sato, *Chem. Mater.* 14, 419 (2002).
24. T. Sasaki, F. Kooli, M. Iida, Y. Michiue, S. Takenouchi, Y. Yajima, F. Izumi, B.C. Chakoumakos, and M. Watanabe, *Chem. Mater.* 10, 4123 (1998).
25. M. Wei, Y. Konishi, H. Zhou, H. Sugihara, and H. Arakawa, *Solid State Commun.* 133, 493 (2005).
26. D.V. Bavykin, J.M. Friedrich, and F.C. Walsh, *Adv. Mater.* 18, 1 (2006).
27. Q. Chen, G.H. Du, S. Zhang, and L.M. Peng, *Acta Crystallogr. Sect. B* B58, 587 (2002).
28. T.P. Feist and P.K. Davies, *J. Solid State Chem.* 101, 275 (1992).
29. X. Sun and Y. Li, *Chem. Eur. J.* 9, 2229 (2003).
30. V. Subramanian, A. Karki, K.I. Gnanasekar, F.P. Eddy, and B. Rambabu, *J. Power Sources* 159, 186 (2006).
31. M. Zukalova, M. Kalbac, L. Kavan, I. Exnar, and M. Graetzel, *Chem. Mater.* 17, 1248 (2005).
32. Q. Wang, Z.H. Wen, and J.h Li, *Inorg. Chem.* 45, 17 (2006).
33. S. Dong, H. Wang, L. Gu, X. Zhou, Z. Liu, P. Ha, Y. Wang, X. Chen, G. Cui, and L. Chen, *Thin Solid Films* 519, 5978 (2011).
34. H. Zhang, G.R. Li, L.P. An, T.Y. Yan, X.P. Gao, and H.Y. Zhu, *J. Phys. Chem. C* 111, 6143 (2007).
35. R.B. Khomane, *J. Colloid Interface Sci.* 356, 369 (2011).
36. Q. Wang, Z. Wen, and J. Li, *Inorg. Chem.* 45, 6944 (2006).